Control of pre-existing fabric in fracture formation, reactivation and vein emplacement under variable fluid pressure conditions: An example from Archean Greenstone belt, India.

Sreyashi Bhowmick and Tridib Kumar Mondal

Department of Geological Sciences, Jadavpur University

5   Kolkata-700032, West Bengal, India

*Corresponding author: **Tridib Kumar Mondal (tridibkumarmondal@gmail.com)**

Alternate E-mail: **tridibk.mondal@jadavpuruniversity.in**

Abstract

10   Most of the upper crustal fluid flows are strongly influenced by the pre-existing fractures/foliations in the rocks under a certain state of tectonic stress and fluid pressure condition. In the present study, we analyze a wide range of crosscutting fractures that are filled with quartz veins of variable orientations and thicknesses, from the gold bearing massive metabasalts (supracrustal) of the Chitradurga Schist Belt adjacent to the Chitradurga Shear Zone (CSZ), western Dharwar craton, south India. The study involves

15   the following steps: 1) analyzing the internal magnetic fabric using anisotropy of magnetic susceptibility (AMS) studies, and strength of the host metabasalts, 2) quantifying the fluid pressure condition through lower hemisphere equal area projection of pole to veins by determining the driving pressure ratio (R´), stress ratio (φ), and susceptibility to fracturing, and 3) deciphering the paleostress condition using fault slip analysis. We interpret that the NNW-SSE to NW-SE (mean 337 °/69° NE) oriented magnetic fabric

20   in the rocks of the region developed during regional D1/D2 deformation on account of NE-SW shortening. However, D3 deformation manifested by NW-SE to E-W shortening led to the sinistral movement along

CSZ. As a consequence of this sinistral shearing, fractures with prominent orientations formed riedel

shear components, with CSZ as the shear boundary. Subsequently, all the pre-existing fabrics along with

the riedel shear components were reactivated and vein emplacement took place through episodic fluid

25 pressure fluctuation from high to low P_f at shallow depth (~2.4 Km). However, NNW-SSE orientations

were susceptible for reactivation under both high and low P_f conditions leading to a much greater

thickness along the same. The deduced paleostress from fault-slip analysis, along with the kinematics of

the fractures and veins are in good agreement with the previously ~~revealed~~ regional tectonics. Thus,

integrating multiple domains of studies, help in the logical interpretation of fluid flow condition and vein

30 emplacement mechanism in the study area that has not been ventured before.

1. Introduction

The upper crust is replete with fractures/faults, which act as pathways for fluid flow and vein

emplacement. Fracture formation and vein emplacement mechanisms are closely interrelated, and require

35 a detailed study for finding out potential hydrothermal deposits. Fracture formation and reactivation

involves a combination of regional stress field (far field stress), stress ratio (Φ) and driving pressure ratio

(R´) that helps to determine the prevailing fluid pressure condition (Delaney et al., 1986; Jolly and

Sanderson, 1997; McKeagney et al., 2004; Mazzarini, 2007; Martinez-Poza et al., 2016; Cucci et al.,

2017). However, previous studies suggest that pre-existing anisotropy in host rocks play a significant role

40 in formation and propagation of fractures provided the anisotropy is favorably oriented to the far field

stresses (Ikari et al., 2015; Donath, 1961; Hoek, 1964; Attwell and Sandford, 1974). Presence of such

favorably oriented anisotropy lowers the shear strength of the host rocks, enabling failure/slip along them at minimum compressive stress, prior to/during vein emplacement. Such conduits are reactivated at both high and low fluid pressures forming pathways for fluid flow (Mondal and Mamtani 2013, Lahiri and

45 Mamtani, 2016). Thus, vein emplacement mechanism requires fracture ~~orientations~~ that can be reactivated, when fluid pressure gradually builds and exceeds the normal stresses acting on the fracture wall (Gudmundsson, 2011). This enables dilation of the fracture ~~planes,~~ a mechanism known as *fault-valve action* (Sibson et al., 1988; Sibson, 1992, 1996, 2000; Boullier and Robert, 1992; Sibson and Scott, 1998; Petit et al., 1999; Cox et al., 2001 among others). Subsequently, fluid flows into the fractures, a

50 phenomenon analogous to *burping*, triggering an immediate drop in fluid pressure. This sudden drop in fluid pressure is responsible for mineral deposition and vein formation (Cox et al., 1991, Cox, 1995; 2001). Vein materials thus deposited seals the fracture/fault planes, preparing the system for the next cycle of fluid pressure build up, rupture, fluid flow and vein formation (Mondal and Mamtani, 2013; Lahiri and Mamtani, 2016; Marchesini et al., 2019). Thus, repeated cycles of elevated and depleted fluid

55 pressure generate criss-cross pattern in veins. Such intricate studies regarding the mechanism of fabric development and fracture formation vis-à-vis vein emplacement helps to provide a detailed insight about the development of brittle structures and their role in understanding the tectonic evolution of Archean cratons.

The Chitradurga Schist belt (western Dharwar craton, south India), is a NW-SE trending Archean

60 greenstone belt, known to harbor a widespread network of veins with potential epigenetic gold bearing lodes (Gupta et al., 2014;Gopalakrishna et al., 2018). We have conducted this study in the meta-volcanic (metabasalt), hosting quartz veins of variable orientations and thicknesses, in and around Chitradurga

region. We emphasize on understanding the mechanism of vein emplacement under a tectonic environment where propensity of fracture reactivation for vein emplacement is mutually dependent on both fluid pressure condition and the regional far field stresses. The present paper is a comprehensive work which quantifies the fabric in the visually isotropic metabasalts of the Chitradurga Greenstone belt and its role in fracture instigation and in channelizing upper crustal fluids. We also found the reactivation potential of the fractures/faults at variable fluid pressure conditions to investigate the role of fractures/faults which are not favorably oriented to the pre-existing anisotropy and regional stress field, and their contribution towards vein emplacement in the study area.

2. Geology of the study area

The study has been conducted in the Chitradurga Greenstone Belt of Dharwar craton (southern India; Fig. 1a), which represents a complex geological history. Dharwar craton exposes >3.0 Ga, Archean continental crusts, represented by the TTG (trondjemite-tonalite-granodiorite gneiss) also known as the peninsular gneiss (Jayananda et al., 2006). The craton stabilized during the accretion of Eastern Dharwar Craton (EDC) and Western Dharwar Craton (WDC) at 2.75-2.51 Ga. The zone of accretion of the two tectonic blocks is marked by a shear zone, referred to as Chitradurga Shear Zone (e.g., Naqvi and Rogers, 1987; Chadwick et al., 2003; Jayananda et al. 2006). The eastern part of WDC marked by Chitradurga Schist Belt (CSB) (Fig. 1b), comprises of peninsular gneiss (3.4-3.0 Ga), and younger supracrustal rocks (Beckinsale et al., 1980; Sarma et al., 2011; Taylor et al., 1984). The latter comprises metavolcanics/metabasalts (greenstone belt; greenschist/lower amphibolite facies metamorphism), metamorphosed greywacke-argillite (interbanded with ferruginous chert and banded iron formation),

polymict conglomerate, and ferruginous chert. It is believed that the basaltic rocks of the schist belt have

85   an island arc affinity (Chakrabarti et al., 2006). Regionally, the belt is surrounded by older peninsular

gneisses and younger granitoids (Ramakrishna and Vaidyanadhan, 2010). Previous geological

investigations, revealed the presence of various younger granites ~2.6 Ga; (Jayananda et al., 2006;

Chardon et al., 2002) which are associated with the schist belt, such as Chitradurga granite, J. N. Kote

granite. The structural investigations of the adjacent meta-sedimentary rocks of the region show that the

90   area has undergone three phases of deformation: D1, D2 and D3 respectively (Chadwick et al., 1989;

Jayananda et al., 2006; Mondal and Mamtani, 2014).The D1/D2 deformations are coaxial with NW-SE

striking axial plane. D1 folds are tight to isoclinal and asymmetric while the D2 folds are open to tight

and upright. Earlier studies revealed that the folds (regional open; NE-SW striking vertical axial plane),

related to early D3 deformation superposed the D1/D2structures thus resulting in dome-basin geometry

95   in the meta-sedimentary rocks of that region (Chakrabarti et al., 2006; Mondal and Mamtani, 2014).

However, later phase of D3 deformation led to the formation of brittle structures in the younger granites

of CSB (Mondal and Mamtani, 2016). The NE-SW shortening during D1/D2 deformation was responsible

for NW-SE oriented structural elements in the CSB (Chadwick et al., 2003), while NW-SE to E-W

shortening direction prevailed during D3 deformation (Jayananda et al., 2006; Mondal, 2018; Mondal and

100   Acharyya, 2018).A number of petrological and geochemical investigations have been carried out on the

area in the past. These studies suggest the presence of actinolite, albite, chlorite, epidote, quartz and calcite

in the basaltic rocks (Chakrabarti et al., 2006). The CSB holds evidence of progressive metamorphism

with a gradual increase in P-T conditions (approximately 3-4 Kb of pressure), from greenschist facies in

north to amphibolite facies in south suggesting the depth of deformation to be 10-12 Km (during D1/D2).

105 However, recent studies by Acharyya and Mondal, (2019) shows that the brittle deformation during late
D3 took place at a shallow depth of ~2-4 km. The dashed rectangular area in figure 1b demarcates the
study area. The present study focuses on the dark greyish to blackish, massive to fine grained, altered
metabasalt hosting quartz veins, of the region surrounded by meta-sedimentary sequences (Fig. 2).The
metabasalts of the study area are devoid of any well-defined ~~field~~ foliation. The foliation planes in the
110 adjacent meta-sedimentary rocks of the region are found to be NW-SE oriented (mean strike/dip is
323º/71º NE). Since, the metabasalts are devoid of mesoscopic field fabric, the anisotropy of magnetic
susceptibility (AMS) study has been conducted in order to quantify ~~the~~ internal magnetic fabric ~~in them.~~

3. Overview of brittle structures

115 Metabasalts of the study area are replete with fractures and faults of multiple orientations. Some of these
fractures and faults are found to host quartz veins forming criss-cross pattern (Fig. 3a and c) and some of
them are devoid of any vein material. Growth of vein materials (quartz crystals) are often found to be
perpendicular to the vein wall suggesting that dilation was significant in these veins (Fig.3b). The
maximum width and length of the quartz veins are ~~recorded to be~~ ~1 meter and ~130 meters respectively.
120 Some of the quartz veins are found to be displaced by other ones forming crisscross network of veins in
the study area (Fig. 3c). Wing cracks filled up with quartz veins are commonly observed (Fig. 3d). At few
places, the thicker quartz veins are replete with series of successive fault planes with slickenside lineations
on them (Fig. 3e and *in-set*). Those veins are often found to enclose angular metabasalt enclaves (host
material, Fig. 3f), suggesting that fault valve action was predominant in the region. Some of the fault
125 planes recorded in the study area have shallow plunging slickenside lineations while others have moderate

to high. Both Left Lateral Faults (LLF's) and Right Lateral Faults (RLF's) are recorded based on the movement of the hanging wall with respect to the footwall. Presence of congruous steps helps in the discrete identification of the fault planes (Fig. 3g). Although, quartz veins of variable orientations and thicknesses are found, however, most of the veins are predominantly NNW-SSE trending (Fig. 4a). Most

130 of the fractures and faults show NNW-SSE trend (maxima) whereas some others form a WNW-ESE to NE-SW sub maxima respectively (Fig. 4b & 4c). Some WNW-ESE trending Mode-I (tensional) cracks with prominent tips are also recorded from the study area which are often filled up with quartz veins. It may be noted that the veins with maximum thicknesses are oriented along NNW-SSE direction (Fig. 4d). In this study, 992 fracture data (strike/dip), 378 vein data (strike, dip and thickness) and 73 fault data

135 (strike, dip and slip) have been measured from the metabasalt exposures ~~of~~ about 13 locations in the entire study area. All 73 shallow to moderately plunging fault planes are used to decipher the paleostress condition. Thus, ~~integrating~~ field observations ~~and data obtained from brittle structures~~ ~~enables to~~ ~~reconstruct the tectonic stress conditions of the craton and~~ helps to quantify the fluid pressure conditions that prevailed during fracture reactivation and vein emplacement.

140

4. Methods of analysis and results

The quartz veins have been emplaced in the massive metabasalts of the region that are devoid of any prominent mesoscopic foliation as mentioned above. At places, veins of one orientation are dissected and sometimes displaced by others that led to the formation of mesh like structures (Fig. 3a, c). Sibson

145 (1992) has mentioned that such a mesh is formed when a rock contains fractures of varying orientations that may get reactivated due to rise in fluid pressure. It is mentioned that in the Chitradurga region, veins

of various orientations show mutually cross-cutting relationships, which implies repeated cycles of vein emplacement (see sect.-3 and Sibson, 1992). Although veins have various orientations, NNW-SSE striking veins are the most common (Fig. 4a). It may be noted that NW-SE to NNW-SSE direction, which

150 defines the maximum strike orientation of quartz veins, fractures and faults, is also the orientation of the adjacent Chitradurga shear zone, the overall trend of the schist belt. This implies that there is a strong structural control on the formation of these quartz veins. It has been shown earlier that the pre-existing anisotropy plays a critical role in propagating fractures and channelizing fluid in rocks (Sanderson and Zhang, 1999, Cox et al., 2001 and Ikari et al., 2015). It is also known from rock mechanics investigations

155 that the rock strength variation controls the strain partitioning and influences fluid flow (e.g., Tsidzi, 1990; Vishnu et al 2018). Therefore, it is crucial to determine the rock fabric and state of stresses in order to understand the upper crustal fluid flow vis-à-vis vein formation.

In the past, 3-D Mohr circle analysis has been performed by Jolly and Sanderson (1997) using dyke orientation data to examine the magma pressure condition that was responsible for the opening of pre-

160 existing fractures during dyke emplacement. Further the work has been extended to understand the fluid pressure condition and vein emplacement mechanism by McKeagney et al., 2004 (also see Yamaji et al., 2010).We present vein orientation data from the Chitradurga region (southern India), which is a province of epigenetic gold deposit (Gupta et al., 2014;Gopalakrishna et al., 2018).

We conduct anisotropy of magnetic susceptibility (AMS) study, followed by Brazilian Tensile

165 strength (BTS) determination in order to quantify the internal magnetic fabric and tensile strength of the rocks within the study area. The 3-D Mohr circle construction using quartz vein orientation data helps to recognise the fluid pressure conditions under which they were emplaced. Further, these fluid pressure

conditions were integrated with dilation tendency, slip tendency and fracture susceptibility in order to understand the mechanism of vein emplacement in the Chitradurga region. A combination of data

170 obtained from these methods along with paleostress analysis using fault-slip data recorded from the study area provides a comprehensive evaluation of vein forming conditions in Chitradurga greenstone belt.

4.1 Anisotropy of Magnetic Susceptibility (AMS)

The quartz veins occur in massive metabasalt, which does not show any visible field foliation.

175 However, such visibly massive rocks may preserve an internal fabric, which can be recognized on the basis of anisotropy of magnetic susceptibility (AMS) studies (e.g., Tarling and Hrouda, 1993; Maffione et al., 2015; Mamtani and Greiling, 2005; Raposo et al., 2007; Loock et al., 2008; Mondal and Mamtani, 2014; Mondal, 2018).The study involves preparation of cylindrical core samples (25.4 mm diameter × 22 mm height) from oriented metabasalt blocks. These metabasalt block samples have been collected from

180 13 different locations (Fig. 5) in the study area. The prepared core samples are subjected to an external magnetic field and the induced magnetization for each core sample is measured in different directions. AMS is considered to be a symmetric second-rank tensor, represented by an ellipsoid with three mutually perpendicular ~~stress~~ axes, K_1, K_2 and K_3 respectively where ($K_1 \geq K_2 \geq K_3$). The orientation and magnitude of each of these principle axes are determined in this analysis, where K_1 represents the magnetic lineation,

185 K_3 is the pole to the magnetic foliation (K_1K_2). Using the magnitudes of K_1, K_2 and K_3, several AMS parameters are calculated such as magnetic susceptibility (K_m), magnitude of the magnetic foliation (F) and magnetic lineation (L), degree of magnetic anisotropy (P_j or P´) and shape parameter (T). The formulae for the parameters are given below (after Tarling and Hrouda, 1993; Jelínek, 1981):

$$K_m = (K_1 + K_2 + K_3) / 3 .$$ (1)

190 $$F = (K_2 - K_3) / K_m .$$ (2)

$$L = (K_1 - K_2) / K_m .$$ (3)

$$P_j = \exp \sqrt{\{2 \, [(\eta_1 - \eta_m)^2 + (\eta_2 - \eta_m)^2 + (\eta_3 - \eta_m)^2]\}} .$$ (4)

$$T = (2\eta_2 - \eta_1 - \eta_3) / (\eta_1 - \eta_3) .$$ (5)

Here, $\eta_1 = \ln K_1$, $\eta_2 = \ln K_2$, $\eta_3 = \ln K_3$ and $\eta_m = (\eta_1 . \eta_2 . \eta_3)^{1/3}$. In the above equations, P_j and T give the

195 measure of the eccentricity and shape of the AMS ellipsoid respectively. The value of T ranges between

-1 to +1. Positive and negative values represent oblate and prolate shapes of the AMS ellipsoid (Tarling

and Hrouda, 1993).

AMS measurements have been conducted in the spinner mode (field intensity of 300 Am^{-1}) using

the KLY-4S Kappabridge (AGICO, Czech Republic); see Hrouda et al. (2006) for instrument details. The

200 SUFAR program has been used to calculate the required AMS parameters described above for each

sample. A total of 65 cores are prepared and analysed. The mean value of the AMS parameters at each

location site is calculated using the program Anisoft (version 4.2, AGICO; Jelinek statistics, Jelinek,

1981).It is noted that the K_m varies between 37 and 1280×10^{-6} SI units, with most of the samples having

K_m below 1000×10^{-6} SI units (see supplementary sheet-1). This indicates that paramagnetic and

205 ferromagnetic minerals contribute significantly to the AMS. Petrographic studies reveal the presence of

actinolite, hornblende, chlorite, albite, epidote, pyrite which are inferred to contribute to the

susceptibilities recorded in the samples. The P_j lies between 1.003 and 1.539, and the shape of the AMS

ellipsoid is dominantly oblate (positive T values; see supplementary sheet-1). It is noted that the magnetic

foliation (K_1K_2 plane) is consistently NW-SE striking (mean orientation: 337º/69º towards NE; Fig. 5a).
210   The magnetic lineations plunge variably from NNW, through sub-vertical to SSE (Fig. 5b).

4.2 Tensile strength determination

It is known that the dilation occurs in a direction parallel to the minimum compressive principal

stress (σ_3), when the fluid pressure (P_f) exceeds the normal stress acting on the fracture wall.

215   Therefore the fractures may occur at any depth when the effective stress ($\sigma_3 - P_f$) is sufficient to

counteract the tensile strength (T) of the rocks (see Fig.10c; Gudmundsson, 2011). We measure the

tensile strength of the host metabasalts to quantify the P_f that prevailed during vein emplacement in

the region. The measurement of direct tensile strength requires machined specimens and also

involves difficulty in applying tensile load on the cylindrical specimen during analysis. Therefore,

220   tensile strength measurement of rocks using Brazilian test has become imperative in rock mechanics.

Compression-induced extensional fractures are generated in the test which essentially involves line-

loading on a circular disk placed between two platens (Aydin and Basu, 2006; Basu et al., 2013; see

Fig.6).This tensile strength (T) is estimated from the elastic theory (ISRM, 1978; ASTM D3967,

2001):

225   $$T = \frac{2P}{\pi LD} \ .\tag{6}$$

Here, P is peak/failure load, and L and D, are the length and diameter of the disk respectively. For this

analysis, 18 core samples were drilled from metabasalt blocks which were later resized to obtain the

desirable cores for the analysis (length: diameter = 1: 2).The maximum tensile strength of each specimen

at the instance of failure is recorded. The maximum tensile strength for18 samples are averaged out to

230   obtain the approximate tensile strength of metabasalts, which is ~12 MPa. This tensile strength value is

further used for quantifying the P_f in 3D Mohr circle using vein orientation data.

4.4 Fluid pressure determination

Here, we have used the method proposed by Jolly and Sanderson (1997) to quantify the P_f conditions that

235   led to the vein emplacement in metabasalts of Chitradurga region (southern India).We have used the lower

hemisphere equal area projection of the poles to quartz vein data. According to Jolly and Sanderson

(1997), girdle distribution of vein pole data implies $P_f > \sigma_2$, described as a condition where large number

of fracture orientations are susceptible to reactivate, while $P_f < \sigma_2$, represents clustered distribution of vein

pole data, where only limited range of fracture orientations reactivate. Depending on the type of

240   distribution (girdle/cluster), parameters such as stress ratio (ϕ) and driving pressure ratio (R´) are

calculated using ranges of fracture orientations (θ_1, θ_2 and θ_3) from the following equations provided by

Jolly and Sanderson, 1997 and Baer et al., 1994.

$$R' = \frac{P_\text{f} - \sigma_3}{\sigma_1 - \sigma_3} = \frac{1 + cos\,2\theta_2}{2}. \qquad (7)$$

For $P_f > \sigma_2$,

$$\Phi = \frac{\sigma_2 - \sigma_3}{\sigma_1 - \sigma_3} = 1 - \frac{1 - cos\,2\theta_2}{1 - cos\,2\theta_3}. \qquad (8)$$

For $P_f < \sigma_2$,

$$\Phi = \frac{\sigma_2 - \sigma_3}{\sigma_1 - \sigma_3} = \frac{1 + cos\,2\theta_2}{1 + cos\,2\theta_1}. \qquad (9)$$

In figure 7a, the lower hemisphere equal area projection of pole to vein data shows girdle distribution,

implying high fluid pressure condition($P_f > \sigma_2$). From this distribution the orientations of the principle

250   stress axes (σ_1, σ_2 and σ_3) are determined using the Bingham statistics of the Stereonet 9 software

(**http://www.geo.cornell.edu/geology/faculty/RWA/programs/stereonet.html**). σ_1 is sub-vertical lying

in the empty space devoid of any vein pole data. Subsequently, following Jolly and Sanderson (1997), the

planes $\sigma_1\sigma_2$, $\sigma_1\sigma_3$ and $\sigma_2\sigma_3$ are constructed and the range of fracture orientations, θ_2 and θ_3 are determined

along the $\sigma_1\sigma_3$ and $\sigma_1\sigma_2$ planes respectively. For this high P_f condition, $\theta_2 = 27º$, $\theta_3 = 59º$ from which $\phi = $

255   0.72 and R´ = 0.8 are calculated. Thus, such a P_f condition enhances the chances of vein emplacement

along various orientations. Although pole to vein data represents a girdle distribution pattern, however

the highest density cluster is found around σ_3 axis indicating a number of veins with similar orientations.

This suggests that the vein forming fluid along these orientations must have been channelized through a

pre-existing anisotropy (along a preferred orientation). These data are segregated and plotted separately

260 in the lower hemisphere equal area projection and thus the obtained contour defines the SW cluster (see.

Fig. 7c). The orientations of the principle stress axes (σ_1, σ_2 and σ_3) are determined using the Bingham

statistics of the Stereonet 9 software. Similarly the $\sigma_1\sigma_2$, $\sigma_1\sigma_3$ and $\sigma_2\sigma_3$ planes are constructed and the

range of fracture orientations θ_1 and θ_2, are calculated along the $\sigma_2\sigma_3$ and $\sigma_1\sigma_3$ planes. Again, for low P_f

condition, $\theta_1 = 38º$, $\theta_2 = 43.2º$, $\phi = 0.85$ and $R´ = 0.53$. This implies that under low fluid pressure condition

265 ($P_f < \sigma_2$) only limited range of fracture orientations are susceptible to reactivate. In each case, for

determining the absolute P_f magnitude, pole to vein data are plotted in 3D Mohr circles. Recent studies

by Mondal and Acharyya (2018), documented the depth of faulting and fracturing in close vicinity of the

study area (Chitradurga granite) to be ~2.4km. Similar depth of fracturing has also been reported by

Acharyya and Mondal (2019), from the elliptical clasts of conglomerate bed within the Chitradurga schist

270 belt. We have considered this depth for determining the magnitude of the maximum compressive stress

(σ_1) during fracture formation, using $\sigma_1 = h\rho g$, where h = depth of fracturing in metabasalts (~2.4km), ρ =

approximate bulk density of crust (2700 kg/m3), g = 9.8 m/sec2. Therefore, $\sigma_1 \geq 63.5$ MPa, when depth

of fracturing in metabasalt~2.4km. Tensile strength of metabasalt (~12 MPa; obtained from BTS studies)

indicates that the minimum compressive stress (σ_3) has to be $\sigma_3 \geq 12$ MPa. In each case we consider the

275 limiting values for both maximum and minimum compressive stresses. Magnitude for the intermediate

compressive stress (σ_2) is determined using the respective stress ratios (ϕ) for both high and low P_f

respectively. Following Jolly and Sanderson (1997), the 3D Mohr circles are constructed using the above

magnitudes of principle stresses and the angles determining the range of fracture orientations. Thus, well-

defined P_f lines for both high P_f (P_f=53.2 MPa; Fig. 7b) and low P_f (P_f=39.3 MPa; Fig. 7d) conditions are

280   obtained using the Fractend code (Github, 2017).

4.5. Dilation tendency, slip tendency and fracture susceptibility

Dilation tendency (T_d) and slip tendency (T_s) determine the propensity of any fracture orientation to

reactive through dilation or shearing, under a certain state of stress condition

285   (Mazzarini, 2019). While, high dilation tendency ensures reactivation through dilation, high slip tendency

elevates chances of opening through shearing (Ferrill et al., 1999). According to, Stephens et al., 2017,

fracture planes suffer dilation when the difference between σ_1 and the normal stress acting on the plane

is close enough to the magnitude of differential stress(σ_D= $\sigma_1 - \sigma_3$) and T_d= ($\sigma_1- \sigma_n$)/ σ_D. Slip tendency is

denoted by the ratio of shear stress (σ_s) to normal stress (σ_n); (T_s= σ_s/σ_n) and also depends on the frictional

290   characteristics of the rock (Morris et al., 1996), along with the fracture plane orientation. Under a

particular state of stress condition if the ratio of shear stress to normal stress is significantly large, then

that particular fracture orientation is susceptible to reactivate. Fracture susceptibility (S_f), is defined as

the variation of fluid pressure (ΔP_f) within a fracture plane that can lead to fluid induced shear reactivation

(Mildren et al., 2002; Stephen et al., 2017). Such reactivations depend on the shear and normal stresses

295   acting on the fracture plane, along with the cohesion (= 0 in this case) and the static coefficient of friction

(μ_s); $S_f = \sigma_n - (\sigma_s/\mu_s)$.

Lower hemisphere equal area projections (see Fig. 8) of the poles to fracture (vein-filled) data help us to

understand the variation in dilation tendency, slip tendency and susceptibility of fractures with respect to

their orientations, under both high and low P_f conditions. The diagrams are prepared using Fractend code

300 (Github, 2017). It is evident from figure 8a, that the dilation tendency is high for the fracture orientations

which are at a high angle to the σ_3 axis, i.e., pole to these fractures form a well-defined cluster around σ_3.

These fractures show greater tendency towards dilational opening for both high and low P_f (Fig. 8a and

b). For fracture orientations having higher slip tendency, i.e., susceptible to shear opening, pole to the

fractures are at a low angle to the σ_3 axis. The fracture planes are therefore oriented at an angle to the

305 maximum compressive stress axis σ_1, condition favorable for shear reactivation for both, high and low P_f

(Fig. 8c and d). Fracture susceptibility, which involves variation in fluid pressure (ΔP_f) is low for the

fracture orientations having high dilation and slip tendencies, which indicates fluid-induced fracture

reactivation in metabasalts (Fig. 8e and f) in the study area.

4.6Paleostress analysis

The shallow to moderaly plunging normal faults of the study area with prominent slip directions are used

to determine the stress regime under which these fractures and faults were formed and reactivated. Fault-

slip data (orientations of fault planes and slip directions) recorded from the field were used for paleostress

determination. Several methods are proposed for paleostress analyses using fault-slip data (e.g. Angelier,

315 1994; Dupin et al., 1993; Etchecopar et al., 1981; Gapais et al., 2000; Marrett and Allmendinger, 1990;

Ramsay and Lisle, 2000; Twiss and Unruh, 1998; Yamaji, 2000; Žalohar and Vrabec, 2007 and the

references therein). Since, the fault-slip analysis methods are well established, here we prefer to represent

only the salient aspects. The fault-slip analysis can be divided into two categories based on whether the

fault-slip data are viewed as representing kinematic or dynamic information (Blenkinsop 2006; Gapais et

320 al. 2000; Twiss & Unruh,1998) based on the following assumptions: (1) bulk state of stress is uniform

and movement on the fault planes are independent of each other; (2) slip on the fault plane occurs along the direction of the maximum resolved shear stress under a given stress state (Wallace–Bott Hypothesis); (3) faults are homogeneous and a part of the same tectonic event (Angelier, 1994; Gapais et al., 2000; Gephart & Forsyth, 1984; Twiss & Unruh, 1998). In this study, we have determined the paleostress direction, using fault-slip data measured from 73 shallow to moderately ~~plunging~~ normal faults (spatially distributed)in the metabasalt by Right Dihedron method. Since, some of the fault planes show variation in their strike orientations, the small amount of inhomogeneity in the data set is reduced in this process. Thus, the data sets are segregated methodically into homogeneous data subsets using the 'Win_Tensor' software program (version 5.8.6; Delvaux and Sperner, 2003; Delvaux, 2011). In the present analysis all the collected data are represented in a single set and separation is done by using the Right Dihedron method without any sort of manual intervention. Following Delvaux and Sperner, 2003, the data is filtered on the basis of stress ratio (R), orientation of the stress axes and symmetry of the measured sets. Out of 73 data, 30 data are accepted with a low value of counting deviation and nominal counting values of 0 and 100 for σ_1 and σ_3 respectively. Thus, the best fitted reduced stress tensor is obtained for the accepted data subset (30 out of 73 fault data; see Fig. 9) at a "C" quality ranking. It also provides the relative orientations of the principal stress axes, stress ratio (R= 0.72) and stress regime index (R´=1.25).The NNE-SSW directed extension direction obtained from this paleostress analysis (see Fig. 9) coincides well with the regional D3 extension direction. Data rejected in this process to obtain the best fit stress tensor when treated separately yields a NNE-SSW oriented extension direction with small variations in the R

340 and R´ values. According to Delvaux and Sperner (2003), the obtained stress regime index indicates a

pure-strike slip domain which is in a good agreement with sinistral shearing along CSZ.

5 Discussions

5.1 Fabric development vis-à-vis regional tectonics

345 It has been mentioned earlier that the metabasalts of the study area lack any distinct visible foliation.

However, the AMS analysis suggests, a prominent NNW-SSE to NW-SE oriented magnetic fabric in

metabasalts. This magnetic fabric also matches well with the field foliation of the meta-sedimentary

sequences, surrounding the metabasalts and is also parallel to the regional trend of CSZ (see Fig. 2).This

implies that the fabric in metabasalts of the study area must have been controlled by the regional

350 deformation. Structural investigations suggest that the Chitradurga region was subjected to three

deformational events-D1, D2 and D3 respectively. D1 and D2 were found to be coaxial and controlled by

NE-SW shortening that led to the development of folds (NW-SE striking vertical axial plane), while D3

was controlled by NW-SE to E-W shortening, resulting in the development of NE-SW striking planar

structures (Chakrabarti et al., 2006; Ramadass et al., 2003). The superposition of D3 over D1/D2 formed

355 culmination and depression in the region (dome-basin structures; Type-I interference pattern)

(Chakrabarti et al., 2006).Therefore, it is logical to infer that the magnetic fabric in metabasalts are also

related to the regional D1/D2 deformation under NE-SW directed shortening that generated the field

foliation in the meta-sedimentary sequences. The magnetic lineations in the metabasalts are plunging due

NNW through sub-vertical to SSE (Fig. 5b).Earlier, these variations in the plunge of the magnetic

360 lineations had been interpreted as a consequence of superposed deformation (e.g., Mamtani and Sengupta,

2010; Mondal and Mamtani, 2013). Therefore, in the light of regional structural information and above discussions, it is inferred that these variations in magnetic lineations of the metabasalts are the manifestation of dome-basin geometry that were produced due to the superposition of D3 over D1/D2 regional deformation. Recently, Mondal (2018) documented similar results from the magnetic fabric

365 analysis in adjacent Chitraurga granite. The studies by Bhatt et al., (2017); Mondal and Acharyya (2018), suggest that the D1/D2 deformation lasted between 2614 and 2555 Ma while the D3 deformation is approximated around ~2537 Ma.

5.2 Control of regional far-field stress on developing the brittle structures in Chitradurga region.

370 The above discussions suggest that (a) NNW-SSE oriented magnetic foliation developed during D1/D2 deformation under NE-SW directed shortening, (b) variation in plunge of magnetic lineation is a manifestation of dome-basin geometry on account of D3 deformation. It is argued that during D3 deformation under NW-SE to E-W directed shortening the CSZ evolved as a sinistral shear zone (Mondal and Acharyya, 2018). It may be noted that the angle between the mean orientation of the schist belt and

375 the compression direction for D3 deformation are found to be ~45° which also supports the sinistral movement along Chitradurga shear boundary.

It is mentioned in ~~sect,~~ 2 and 3 that, the study area is replete with a number of brittle structures such as fractures, faults. At places, these fractures are filled-up with quartz veins ~~and the present paper is aimed to understand the mechanism behind the formation of these veins.~~ Therefore, it is now essential to

380 evaluate whether and how this brittle structures and their kinematics can be fitted to the regional far-field stresses responsible for deformation in the Chitradurga region. The quartz vein orientation data from

northern part of the Chitradurga schist belt reveals that the vein emplacement took place during regional

D3 deformation (Mondal and Mamtani, 2014). Recently, Mondal andAcharyya (2018), and Acharyya and

Mondal (2019) suggested that the brittle structures (fractures/faults) in the Chitradurga granite (in close

385   vicinity to the study area) are related to the D3 deformation.Moreover, paleostress investigation using

fault-slip data also reveals NNE-SSW directed extension was dominant during D3 deformation. Apart

from this, evidences of any later deformation, i.e., post D3 deformation, have not been recorded from the

study area (from previous studies and as per our field observations). Thus, based on the present studies

and above discussions, it is logically inferred that the formation of brittle structures (fractures/faults) as

390   well as vein emplacement must be explained as a consequence of regional D3 deformation at a shallow

depth. Mondal and Mamtani (2014) suggested that the Mulgund granite (2555 ± 6 Ma; Sarma et al., 2011),

which lies in close vicinity to the metabasalts of the Chitradurga region, was emplaced syn-tectonically

with CSZ. It is shown that the Mulgund granite underwent ductile deformation as it cooled and

crystallized syntectonically with D3 deformation. The ductile deformation features in the granite were

395   then superimposed by brittle structures during late D3, when the granite was fully solidified and had

achieved a shallow depth (Mondal and Mamtani, 2016).Since both the lithologies (metabasalts and

granite) have undergone same deformation and the fractures in them developed syntectonically with

adjacent CSZ, it is favourable to interpret that the brittle structures, such as fractures and faults in

metabasalts developed on account of late D3 deformation under NW-SE to E-W directed compression at

400   a shallow depth of about ~ 2.4 Km. For evaluating the nature (mode) of fracturing in the metabasalts of

the study area, we used tensile strength (T) to be12 MPa (from BTS studies). We estimated $\Delta\sigma$= 51.5

MPa, which is greater than 4T, suggesting that the fractures in the metabasalts are not purely tensile except

for the cracks parallel to D3 shortening direction. However, the calculated value of Δσ is less than 5.7T,

indicating that the normal stress on the fractures are not purely compressive also. Therefore the value of

405   Δσ satisfies 4T $<\sigma_1 - \sigma_3 <$ 5.7 T (Sibson, 2000), indicating that these fractures in the study area are

extensional shear mode fractures**.**

5.3 Regional tectonics and the mechanism of fracturing, faulting

We discussed earlier in sect. -3, that the fractures and faults recorded in the metabasalts show a wide

410   range of orientations with a NNW-SSE maxima and a WNW-ESE to NE-SW sub-maxima respectively

(Fig. 4b).Among which, fractures trending along WNW-ESE to E-W are sub-parallel to the D3 (late

phase) shortening direction. As previously mentioned in sect. -3, these WNW-ESE trending fractures

have been regarded as tensional fractures. Similar orientations have also been recorded and interpreted as

tensile fractures from the micro-granitoid enclaves in Chitradurga granite as evident from the studies of

415   Mondal and Acharyya (2018). However, it is essential to explain the predominance of fractures and faults

along the NNW-SSE orientation (forming the maxima). In order to explain this, we refer to the pre-

existing fabric in the metabasalts of the study area, i.e., the NNW-SSE to NW-SE oriented magnetic fabric

developed during D1/D2 regional deformation (Fig. 5a). Earlier studies suggest, that fractures are more

likely to propagate along a pre-existing anisotropy, if and when the anisotropy is favorably oriented with

420   respect to the regional stress field (Ikari et al., 2015). The CSZ being a sinistral shear zone exhibits a pure

strike slip stress regime, coeval with D3 deformation (NW-SE to E-W directed shortening).

 In the later phase of D3 deformation, the favorably oriented NNW-SSE fabrics were reactivated under a

congenial stress field, thereby, causing reactivation of the pre-existing fabrics in the metabasalts. This

however, fails to justify the occurrence of the ~NW-SE and ~NE-SW oriented fractures within the
metabasalts. From field investigations, the NE-SW oriented fractures show dextral movements, while the
NNW-SSE and NW-SE oriented fractures are recorded with sinistral movements respectively (see Fig.
3c and d). However, the fracture disposition and consistency in their respective orientations indicate that
all of these fractures are related to the same deformational event and have been reactivated under similar
stress conditions. Moreover, any other brittle deformational event post D3, have not been recorded from
the study area as mentioned earlier. Therefore, we need to explain the occurrence of such variably oriented
fractures/faults within a single kinematic framework. The NNW-SSE and NW-SE orientations are most
likely to be sinistral, whereas NE-SW orientations form the dextral shear components respectively,
considering CSZ to be the sinistral shear boundary. (See Fig. 10b and 4b, c). Thus, the NNW-SSE to NW-
SE (P, Y and R) and the NE-SW to ENE-WSW (X and R′) fractures coincide with the shear components
of a riedel shear system considering the angle of internal friction (Φ) in metabaslts of the study area to be
~30˚. It may be noted that the value of Φ is approximated from the Uniaxial Compressive Strength (UCS)
studies of the metabasalts core samples following Sivakugan et al., 2014. These fracture planes acted as
pathways for fluid flow and vein emplacement during the late D3 deformation.

5.4 Understanding the mechanism of fluid flow and vein emplacement in Chitradurga region

In order to explain the vein emplacement mechanism along these weak zones we need to consider the
fluid pressure conditions that prevailed in the study area. In sect. 4.4, we mentioned earlier that the lower
hemisphere equal area projection of pole to vein data shows girdle distribution, indicating high P_f
condition (~53.2 MPa; >σ_2) in the study area. Under such high P_f conditions, veins were emplaced along

445   all possible orientations, including NNW-SSE, NW-SE, WNW-ESE, NE-SW and ENE-WSW trending

fractures. The building fluid pressure surpassed the normal stresses acting on the fracture wall, and hence,

fluid burped into the weak planes leading to fluid-induced reactivation of the fractures, promoting vein

emplacement along them (Fig. 10c).However, the NNW-SSE trending veins show greater thickness and

abundance with respect to other orientations (see Fig. 4d and 3e). We found that pole to these veins

450   (NNW-SSE trending orientations) lie within the warm zones of the stereoplots obtained from the Fractend

code (Github, 2017), indicating higher dilation tendencies (see Fig. 8a and 8b). In Fig. 8a and 8b, it is

perceived that pole to these orientations form a cluster around the σ_3 stress axis. Similarly, pole to the

orientations trending NW-SE and NE-SW respectively, have higher slip tendencies, indicating shear

reactivation along them (Fig. 8c and d). Most of the poles to the NNW-SSE trending orientations lie

455   within the overlapping warm zones, indicating high potential to reactivate in both shear and dilation mode

(high slip and dilation tendencies). These orientations are susceptible for dilation as well as shear

reactivation, depending on the predominance of fluid pressure and availability of fluid for inducing

dilation or shear reactivation. Availability of fluid significantly reduces the effective normal stress (σ_n'

$=\sigma_n$- P_f); where σ_n' and σ_n are the effective normal stress and normal stress respectively) acting on the

460   fracture planes (see Fig. 10c and d). Under this condition, fluid burps into the fractures leading to a

significant drop in the fluid pressure. This sudden drop in the fluid pressure reduces the solubility of fluid

materials promoting deposition of vein followed by sealing of the pathways (Cox et al., 1991, 2001).

Pathways thus remains sealed till the next cycle of fluid pressure build up, fracture reactivation and vein

deposition. However, in between two such cycles of high fluid pressure, an intermediate low fluid

465   pressure cycle persists, during which fluid pressure might not be substantially high to reactivate all the

pre-existing pathways. Thus, a high fluid pressure cycle is followed by a subsequent pulse of low fluid

pressure causing selective reactivation of some of the pre-existing orientations. Hence, it is envisaged

that, these cycles of high and low P_f conditions might have been repeated multiple times (n-times) until

the fluid source was completely exhausted. In the present case, the low P_f condition is interpreted by

470   discretely analyzing the cluster within the girdle distribution of pole to vein data in the lower hemisphere

equal area projection. (see sect. 4.4). Such low P_f could not surpass the normal stresses of all the pre-

existing pathways. And only the NNW-SSE oriented ones (related to the magnetic fabric of the

metabasalts) having high dilation and slip tendencies were favorably oriented for reactivation and fluid

flow. The above mechanism of *fault-valve action* is supported with field evidences showing occurrences

475   of thick quartz veins enclosing angular chunks of metabasalt hosts with multiple sub-parallel fault planes

(identified from the slickenside lineations), see Fig. 3d & 3e. This suggests that the process of fracturing,

fracture reactivation through faulting and vein emplacement (*fault-valve* action) prevailed throughout the

D3 deformation. Thus, the process of new fracture formation and reactivation were continuously

persistent during the entire late D3 phase, with intermittent episodes of vein emplacement under both high

480   and low P_f conditions.

7 Conclusions

In the present study, we commented on the vein emplacement mechanism of the Chitradurga greenstone

belt (Dharwar craton, south India). We analysed the magnetic fabric data recorded from AMS analysis of

485   the metabasalt that hosts the quartz veins. 3D Mohr circle and paleostress analysis have been used to

evaluate the vein emplacement vis-à-vis regional deformation. Following are the main findings and conclusions from the study:

1. The NW-SE oriented magnetic fabric recorded in the metabasalts (as evident from the AMS analysis) is a product of the D1/D2 regional deformation on account of NE-SW directed shortening. This fabric was also favourably oriented and therefore, suitable for fracture propagation in relation to the prevailing stress field.

2. D3 deformation manifested by NW-SE to E-W directed shortening was coeval with the sinistral movement along CSZ. It is concluded that during late D3 deformation all pre-existing fabrics and the ones constituting the riedel shear system were reactivated, with CSZ acting as a shear boundary.

3. The variably oriented fractures and faults i.e., the NNW-SSE, NW-SE, WNW-ESE, NE-SW and ENE-WSW oriented ones are identified as the P, Y, R, T, X and R´ shear components of the riedel shear system. The NNW-SSE oriented shears (P, Y and R) are abundant owing to their favourable correspondence with the pre-existing AMS fabric.

4. Paleostress analysis using fault-slip data recorded from field studies reveals NNE-SSW directed extension, asserting reactivation under a WNW-ESE directed compression (related to D3 deformation).

5. Vein emplacement took place under both high and low P_f conditions. It is envisaged that multiple number of such alternating high and low P_f cycles prevailed in the process of fluid flow and vein emplacement in the region.

6. Vein emplacement took place along all possible orientations. Evidences of *fault-valve behaviour* and fluid induced fracture/fault reactivation have been recorded from field studies. However, the NNW-SSE trending orientations having higher values of slip and dilation tendencies, channelized fluid during both high and low P_f conditions, thereby attaining maximum vein thickness.

7. The process of fracture formation, reactivation and faulting prevailed under a far field compression related to late D3 deformation. However, intermittent episodes of fluid pressure build up led to fluid induced faulting, rupturing and vein emplacement in the region.

Author contribution: SB: conceptualization, methodology, data curation, formal analysis, writing. TKM: supervision, conceptualization, methodology, data curation, funding acquisition, writing.

Competing interests: The authors declare that they have no conflict of interest.

Acknowledgments

The study is funded by DST-SERB (File No. ECR/2015/000079) and RUSA 2.0 to TKM. This study is a part of SB's doctoral research; being funded by DST Inspire (IF170912). Geological Survey of India (Bangalore) is acknowledged for helping with logistic support and discussions during fieldwork. Prof. Manish A. Mamtani is thanked for allowing the authors to use KLY-4S Kappabridge system (IIT Kharagpur, India) for AMS analysis. Prof. Arindam Basu and Dr. Bikash K. Ram are thanked for helping

525 with tensile strength measurements using GCTS$^{©}$ at IIT Kharagpur, India. Assistance provided by Ayan

Patsa, Subha Saha and Swarnasree Mondal are acknowledged.

References

Acharyya, S.S., Mondal, T.K.: Stress enhanced tensile fractures in elliptical clast in conglomerate. Journal
530 of Structural Geology 122 (2019) 81–88, https://doi.org/10.1016/j.jsg.2019.02.001, 2019.

Angelier, J., 1994.: Fault slip analysis and palaeostress construction. In: Hancock, P.L. (Ed.), Continental
 Deformation. Pergamon Press, London.

ASTM (2001) American Society for Testing and Materials. ASTM Standards on Disc, 04.08. West
 Conshohocken, PA, 2001.

535 Attewell, P.B., Sandford, M.R.: Intrinsic shear strength of a brittle, anisotropic
 Rock-I. Experimental and mechanical interpretation. Int. J. Rock Mech. Min.
 Sci. Geomech. Abstract. 11, 423-430, 1974.

Aydin A, Basu A.: The use of Brazilian test as a quantitative measure of rock weathering. Rock Mech
 Rock Eng 39:77–85, https://doi.org/10.1007/s00603-005-0069-0, 2006.

540 Baer, G., Beyth, M., Reches, Z.: Dikes emplaced into fractured basement, Timna Igneous Complex,
 Israel. Journal of Geophysical Research 99, 24039–24051, https://doi.org/10.1029/94JB02161,
 1994.

Basu, A., Mishra, D.A., Roychowdhury, K.: Rock failure modes under uniaxial compression, Brazilian,
 and point load tests. Bull EngGeol Environ (2013) 72:457–475,
545 http://dx.doi.org/10.1007%2Fs10064-013-0505-4, 2013.

Beckinsale, R. D., Drury, S. A., Holt, R. W.: 3305–Myr old gneisses from south

 Indian craton. Nature 283, 469–470, 1980.

Bhatt, S., Rana, V., Mamtani, M.A.: Deciphering relative timing of fabric development in granitoids withsimilar absolute ages based on AMS study (Dharwar Craton, SouthIndia). Journal of Structural Geology 94 (2017) 32-46, https://ui.adsabs.harvard.edu/link_gateway/2017JSG....94...32B/doi:10.1016/j.jsg.2016.11.002, 2017.

Blenkinsop, G. T.: Kinematic and dynamic fault slip analyses: implications from the surface rupture of the 1999 Chi–Chi, Taiwan, earthquake, Journal of Structural geology, 28, 1040–1050, https://doi.org/10.1016/j.jsg.2006.03.011, 2006.

Boullier, A. M., Robert, F.: Palaeoseismic events recorded in Archaean gold quartz vein networks, Val d'Or, Abitibi, Quebec, Canada. Journal of Structural Geology14, 161–179, https://doi.org/10.1016/0191-8141(92)90054-Z, 1992.

Chadwick, B., Vasudev, V. N., Hedge, G. V.: The Chitradurga schist belt and its adjacent plutonic rocks NW of Tungabhadra, Karnataka: a duplex in the late Archean convergent setting of the Dharwar craton. Journal of the Geological Society of India 61, 611–613, 2003.

Chadwick, B., Ramakrishnan, M., Vasudev, V. N., Viswanatha, M. N.: Facies Distributions and Structure of a Dharwar Volcano sedimentary Basin: Evidence for Late Archaean transpression in Southern India? Journal of the Geological Society of London 146, 825–834, 1989.

Chakrabarti, C., Mallick, B. S., Pyne, T. K., Guha, D.: A manual of the Geology of India. Geological Survey of India, Kolkata, 2006.

Chardon, D., Peucat, J.–J., Jayananda, M., Choukroune, P., Fanning, C.M.: Archaean granite–greenstone tectonics at Kolar (south India): interplay of diapirism and bulk inhomogeneous contraction during juvenile magmatic accretion. Tectonics 21, 1–17, https://doi.org/10.1029/2001TC901032, 2002.

Cox, S. F., Knackstedt, M. A., Braun, J.: Principles of structural control on permeability and fluid flow in hydrothermal systems. Society of Economic Geologists Reviews 14, 1–24, 2001.

Cox, S. F.: Faulting processes at high fluid pressures: an example of fault–valve behaviour from the Wattle Gully Fault, Victoria, Australia. Journal of Geophysical Research 100, 12841–12860, https://doi.org/10.1029/95JB00915, 1995.

575 Cox, S. F., Wall, V. J., Etheridge, M. A., Potter, T. F.: Deformational and metamorphic processes in the formation of mesothermal vein–hosted gold deposits — examples from the Lachlan Fold Belt in central Victoria, Australia. Ore Geology Reviews 6, 391–423, https://doi.org/10.1016/0169-1368(91)90038-9, 1991.

Cucci, L., Luccio, F.D., Esposito, A., Ventura, G.: Vein networks in hydrothermal systems provide
580 constraints for the monitoring of active volcanoes. Scientific reports 7:146, https://dx.doi.org/10.1038%2Fs41598-017-00230-8, 2017.

Delaney, P. T., Pollard, D. D., Zioney, J. I., McKee, E. H.: Field relations between dikes and joints: emplacement processes and palaeostress analysis. Journal of Geophysical Research 91 (B5), 4920–4938, **doi.org/10.1029/JB091iB05p04920**, 1986.

585 Delvaux, D.: EGU General Assembly. Win-tensor, an Interactive Computer Program for Fracture Analysis and Crustal Stress Reconstruction, vol. 13 , Geophysical Research Abstract, Vienna, 2011

Delvaux, D., Sperner, B.: Stress tensor inversion from fault kinematic indicators and focal mechanism data: the TENSOR program. In: Nieuwland, D. (Ed.), New Insights into Structural Interpretation
590 and Modelling: Geol. Soc. Lond. Special Publication 212, 75–100, 2003.

Donath, F.A.: Experimental study of shear failure in anisotropic rocks. Geol.

Soc. Am. Bull. 72, 985-990, 1961.

Dupin, J. M., Sassi, W., Angelier, J.: Homogeneous stress hypothesis and actual fault slip: a distinct element analysis, Journal of Structural Geology 15, 1033–1043, doi.org/10.1016/0191-
595 8141(93)90175-A, 1993.

Etchecopar, A., Vasseus, G., Daigniers, M. : An inverse problem in microtectonics for the determination of stress tensor from fault striation analysis, Journal of Structural Geology 3, 51–65, DOI: 10.1016/0191-8141(81)90056-0, 1981.

Ferrill, D.A., Winterle, J., Wittmeyer, G., Sims, D., Colton, S., Armstrong, A., Morris, A.P., 1999.
600 Stressed rock strains groundwater at Yucca Mountain, Nevada. GSA Today 9, 1–8.

Gapais, D., Cobbold, P. R., Bourgeois, O., Rouby, D., de Urreiztieta, M.: Tectonic
Significance of fault–slip data, Journal of structural Geology. 22, 881–888, doi.org/10.1016/S0191-8141(00)00015-8, 2000.

Gephart, J. W., Forsyth, D. W.: An improved method for determining the regional stress tensor using earthquake focal mechanism data: application to the San Fernando earthquake sequence, Journal Geophysical Research 89(B11), 9305–9320, **doi.org/10.1029/JB089iB11p09305**, 1984.

GitHub, 2017. FracTend MATLAB code. https://github.com/DaveHealy-Aberdeen/FracTend

Gopalakrishna, G., Shareef, M., Nagesh, P.C., 2018. Shear-Controlled Gold Mineralization of G. R.Halli Area of Chitradurga Schist Belt, DharwarCraton: Insights from Fluid Inclusion Study. Open Journal of Geology, 8, 662-673, DOI: 10.4236/ojg.2018.87039 , 2018.

Gudmundsson, A., 2011. Rock Fractures in Geological Processes. Cambridge UniversityPress.

Gupta, S.,Jayananda, M., Fareeduddin, 2014. Tourmaline from the Archean G.R. Halli Gold Deposit, Chitradurga Greenstone Belt, Dharwar Craton (India): Implications for the Gold Metallogeny. Geoscience Frontiers, 5, 877-892, doi.org/10.1016/j.gsf.2013.12.004, 2014.

Hoek, E.: Fracture of anisotropic rock. J. South Afr. Inst. Min. Metal. 64 (10), 501-518, 1964.

Hrouda, F., Chlupáčová, M., Pokorný, J.: Low–field variation of magnetic susceptibility measured by the KLY–4S Kappabridge and KLF–4A magnetic susceptibility meter: Accuracy and interpretational programme. Studia Geophysica et Geodaetica 50, 283–299, 2006.

Ikari, M.J., Neimeijer, A.R., Marone, C.: Experimental investigation of incipient shear failure in foliated rock. Journal of Structural Geology 77, 82-91, doi.org/10.1016/j.jsg.2015.05.012, 2015.

ISRM, Suggested methods for determining tensile strength of rock materials. Int. J. Rock Mech. Min. Sci. & Geomech. Abstr., Vol. 15, 99-103, 1978.

Jayananda, M., Chardon, D., Peucat, J.–J., Capdevila, R.: 2.61 Ga potassic granites and crustal reworking
in the western Dharwar craton, southern India: tectonic, geochronologic and geochemical
constraints. Precambrian Research 150, 1–26, DOI: 10.1016/j.precamres.2006.05.004, 2006.

Jelínek, V.: Characterization of magnetic fabric of rocks. Tectonophysics 79, T63–T67,
DOI:10.1016/0040-1951(81)90110-4, 1981.

Jolly, R.J.H., Sanderson, D.J. : A Mohr circle reconstruction for the opening of a   pre-existing fracture.
Journal of Structural Geology 19, 887-892, DOI. 10.1016/S0191-8141(97)00014-X, 1997

Lahiri, S., Mamtani, M.A.: Scaling the 3-D Mohr circle and quantification of paleostress during fluid
pressure fluctuation–Application to understand gold mineralization in quartz veins of Gadag
(southern India). Journal of Structural geology 88, 63–72, doi.org/10.1016/j.jsg.2016.05.003, 2016.

Logan, J. M., Dengo, C. A., Higgs, N. G., Wang, Z. Z.: Fabrics of experimental fault zones: their
development and relationship to mechanical behaviour. In: Evans, B. & Wong, T. (eds) Fault
Mechanics and Transport Properties of Rocks. Academic Press, San Diego, CA, 33–67, 1992.

Loock, S., Diot, H., Van Wyk de Vries, B., Launeau, P., Merle, O., Vadeboin, F., Petronis, M.S.: Lava
flow internal structure found from AMS and textural data: An example in methodology from the
Chaîne des Puys, France. Journal of Volcanology and Geothermal Research 177, 1092–1104,
doi.org/10.1016/j.jvolgeores.2008.08.017, 2008.

Maffione, M., Hernandez-Moreno, C., Ghiglione, M.C., Speranza, F., van Hinsbergen, D.J.J., Lodolo, E.:
Deformation of the Southern Andes since the Late Cretaceous: constraints from anisotropy of
magnetic susceptibility (AMS). Tectonophysics 665, 236–250,
doi.org/10.1016/j.tecto.2015.10.008, 2015.

Mamtani, M.A., Greiling, R.O.: Granite emplacement and its relation with regional deformation in the
Aravalli Mountain Belt–inferences from magnetic fabric. Journal of Structural Geology 27, 2008–
2029, doi.org/10.1016/j.jsg.2005.06.004, 2005.

Mamtani, M.A., Sengupta, P.: Significance of AMS analysis in evaluating superposed folds in quartzites.
Geological Magazine 147, 910–918, DOI: 10.1017/S0016756810000397, 2010

650 Marchesini, B., Garofalo, P.S, Menegon, L., Mattila, J., Viola, G.: Fluid-mediated, brittle–ductile deformation at seismogenic depth –Part 1: Fluid record and deformation history of fault veins in a nuclear waste repository (Olkiluoto Island, Finland). Solid Earth, 10, 809–838, doi.org/10.5194/se-10-809-2019, 2019.

Marrett, R., Allmendinger, R. W.: Kinematic analysis of fault–slip data , J.Struc.Geol. 12, 973–986.
655 doi.org/10.1016/0191-8141(90)90093-E, 1990.

Martínez-Poza, A. I., Druguet, E., Castaño, L. M., Carreras, J.: Dyke intrusion into a pre-existing joint network: The Aiguablava lamprophyre dyke swarm (Catalan Coastal Ranges). Tectonophysics 630, 75–90, doi.org/10.1016/j.tecto.2014.05.015, 2014.

Mazzarini, F., Isola, I.: Hydraulic connection and fluid overpressure in upper crustal rocks: evidence from
660 geometry and spatial distribution of veins at Botrona quarry, southern Tuscany, Italy. Journal of Structural Geology 29, 1386-1399, doi.org/10.1016/j.jsg.2007.02.016, 2007.

Mazzarini, F., Musumeci, G., Viola, G., Garofalo, P.S., Mattila, J.: Structural and lithological control on fluid circulation, dilation and ore mineralization (Rio Albano mine, Island of Elba, Italy). Journal of Structural Geology 126 (2019) 210–230, doi.org/10.1016/j.jsg.2019.06.012, 2019.

665 McKeagney, C.J., Boulter, C.A., Jolly, R.J.H., Foster, R.P.: 3-D Mohr Circle analysis of vein opening, Indarama lode-gold deposit, Zimbabwe: implications for exploration. Journal of Structural Geology 26, 1275-1291, doi.org/10.1016/j.jsg.2003.11.001, 2004.

Mondal, T.K., Acharyya, S.S.: Fractured micro-granitoid enclaves: a stress marker. Journal of Structural Geology 113, 33–41, DOI: 10.1016/j.jsg.2018.05.011, 2018.

670 Mondal, T.K.: Evolution of fabric in Chitradurga granite (south India)-A study based on microstructure, anisotropy of magnetic susceptibility (AMS) and vorticity analysis. Tectonophysics 723, 149–161, doi.org/10.1016/j.tecto.2017.12.013, 2018.

Mondal, T.K., Mamtani, M.A.: Palaeostress analysis of normal faults in granite implications for interpreting Riedel shearing related to regional deformation. Journal of Geological Society 173,
675 216–227, doi.org/10.1144/jgs2014-136, 2016.

Mondal, T.K., Mamtani, M.A.: Fabric analysis in rocks of the Gadag region (southern India)-implications for time relationship between regional deformation and gold mineralization. Tectonophysics 629, 238–249, DOI: 10.1016/j.tecto.2013.09.021, 2014.

Mondal, T.K., Mamtani, M.A.: 3-D Mohr circle construction using vein orientation data from Gadag (southern India) e implications to recognize fluid pressure fluctuation. J. Struct. Geol. 56, 45-56, doi.org/10.1016/j.jsg.2013.08.005, 2013.

Mildren, S.D., Hillis, R.R., Kaldi, J.: Calibrating predictions of fault seal reactivation in the Timor Sea. APPEA J.42 (1), 187–202, 2002

Morris, A., Ferrill, D.A., Henderson, D.B., 1996. Slip-tendency analysis and fault reactivation. Geology 24, 275–278.

Naqvi, S.M., Rogers, J.J.W.: Precambrian geology of India: Oxford monographs on geology and geophysics No. 6. Oxford University Press, New York. 1987

Petit, J. P., Wibberley, C. A. J., Ruiz, G.: `Crack±seal', slip: a new fault valve mechanism? Journal of Structural Geology 21, 1199-1207, 1999, 10.1016/S0191-8141(99)00038-3.

Ramakrishnan, M., Vaidyanadhan, R., 2010. Geology of India. Vol. 1. Geological Society of India, Bangalore.

Ramadass, G., Himabindu, D., Srinivasulu, N., 2003. Structural appraisal of the Gadag schist belt from gravity investigations. Proceedings of the Indian Academy of Sciences (Earth and Planetary Science) 112, 577–586.

Ramsay, J.G. & Lisle, R.J.: The Techniques of Modern Structural Geology. Vol. 3: Applications of Continuum Mechanics in Structural Geology. Academic Press, London, 2000.

Raposo, M.I.B., D'Agrella–Filho, M.S., Pinese, J.P.P.: Magnetic fabrics and rock magnetism of Archaean and Proterozoic dike swarms in the southern São Francisco Craton, Brazil. Tectonophysics 443, 53–71 doi.org/10.1016/j.tecto.2007.08.001, 2007.

Sanderson, D. J., Zhang, X., 1999. Critical stress localization of flow associated with deformation of well–fractured rock masses, with implications for mineral deposits. In: McCaffrey, K. J. W.,

Lonergan, L. and Wilkinson, J. J. (Eds.) Fractures, Fluid Flow and Mineralization. Geological Society of London, Special Publications 155, 69–81.

Sarma, D. S., Fletcher, I. R., Rasmussen, B., McNaughton, N. J., Mohan, M. R., Groves, D. I.: Archean gold mineralization synchronous with late cratonization of the Western Dharwar Craton, India: 2.52 Ga U–Pb ages of hydrothermal monazite and xenotime in gold deposits. Mineralium Deposita 46, 273–288, DOI: 10.1007/s00126-010-0326-3, 2011.

Sibson, R. H.: A brittle failure mode plot defining conditions for high flux–flow. Economic Geology 95, 41–48, 10.2113/gsecongeo.95.1.41, 2000.

Sibson, R. H., Robert, F., Poulsen, K. H.: High–angle reverse faults, fluid–pressure cycling, and mesothermal gold–quartz deposits. Geology 16, 551–555, doi.org/10.1130/0091-7613(1988)016<0551:HARFFP>2.3.CO;2, 1988

Sibson, R. H., Scott, J.: Stress/fault controls on the containment and release of over pressured fluids: examples from gold–quartz vein systems in Juneau, Alaska,Victoria, Australia, and Otago, New Zealand. Ore Geology Reviews 13, 293–306, 10.1016/S0169-1368(97)00023-1, 1998.

Sibson, R. H.: Structural permeability of fluid–driven fault–fracture meshes. Journal of Structural Geology 18, 1031–1043, doi.org/10.1016/0191-8141(96)00032-6, 1996.

Sibson, R. H.: Implications of fault–valve behaviour for rupture nucleation and recurrence. Tectonophysics 211, 283–293, doi.org/10.1016/0040-1951(92)90065-E, 1992.

Sivakugan, N., Das, B. M., Lovisa, J., Patra, C. R.: Determination of c and w of rocks from indirect tensile strength and uniaxial compression tests. International Journal of Geotechnical Engineering 8, 59-65, doi.org/10.1179/1938636213Z.00000000053, 2014.

Stephens, T.L., Walker, R.J., Healy, D., Bubeck, A., England, R.W., McCaffrey, K.J.: Igneous sills record far-field and near-field stress interactions during volcano construction: Isle of Mull, Scotland. Earth Planet. Sci. Lett. 478, 159–174. doi.org/10.1016/j.epsl.2017.09.003, 2017.

Tarling, D. H., Hrouda, F., 1993. The Magnetic Anisotropy of Rocks. Chapman and Hall, London.

Taylor, P.N., Chadwick, B., Moorbath, S., Ramakrishnan, M., Viswanatha, M.N.: Petrography, chemistry and isotopic ages of Peninsular Gneiss, Dharwar acid volcanic rocks and the Chitradurga granite

with special reference to the late Archaean evolution of the Karnataka craton. Precambrian
730   Research 23, 349- 375. 10.1016/0301-9268(84)90050-0, 1984.

Thyng, K.M., Greene, C.A., Hetland, R.D., Zimmerle, H.M., DiMarco, S.F,: True Colors of
Oceanography Guidelines for Effective and Accurate Colormap Selection. Oceanography, 9-13,
doi.org/10.5670/oceanog.2016.66, 2016

Tsidzi, K. E. N.: The influence of foliation on point load strength anisotropy of foliated rocks. Engineering
735   Geology 29, 49–58. 10.1016/0013-7952(90)90081-B, 1990.

Twiss, R. J., Unruh, J. R.: Analysis of fault slip inversions; do they constrain stress or strain rate? , Journal
of Geophysical Research 103 (B6), 12205–12222, **doi.org/10.1029/98JB00612**.1998.

Vishnu, C. S., Lahiri, S., Mamtani, M. A.: The relationship between magnetic anisotropy, rock-strength
anisotropy and vein emplacement in gold-bearing metabasalts of Gadag (South India).
740   Tectonophysics 722, 286-298, doi.org/10.1016/j.tecto.2017.09.011. 2018.

Yamaji, A., Sato, K, Tonai, S.: Stochastic modeling for the stress inversion of vein orientations:
Paleostress analysis of Pliocene epithermal veins in south western Kyushu, Japan. Journal of
Structural Geology 32. 1137–1146. DOI: 10.1016/j.jsg.2010.07.001, 2010.

Yamaji, A.:The multiple inverse methods: a new technique to separate stresses from heterogeneous fault-
745   slip data, Journal of Structural Geology 22, 441–452. DOI: 10.1016/S0191-8141(99)00163-7
2000.

Žalohar, J., Vrabec, M.: Paleostress analysis of heterogeneous fault–slip data: the Gauss method, Journal
of Structural Geology 29, 1798–1810. DOI: 10.1016/j.jsg.2007.06.009, 2007.

750

755
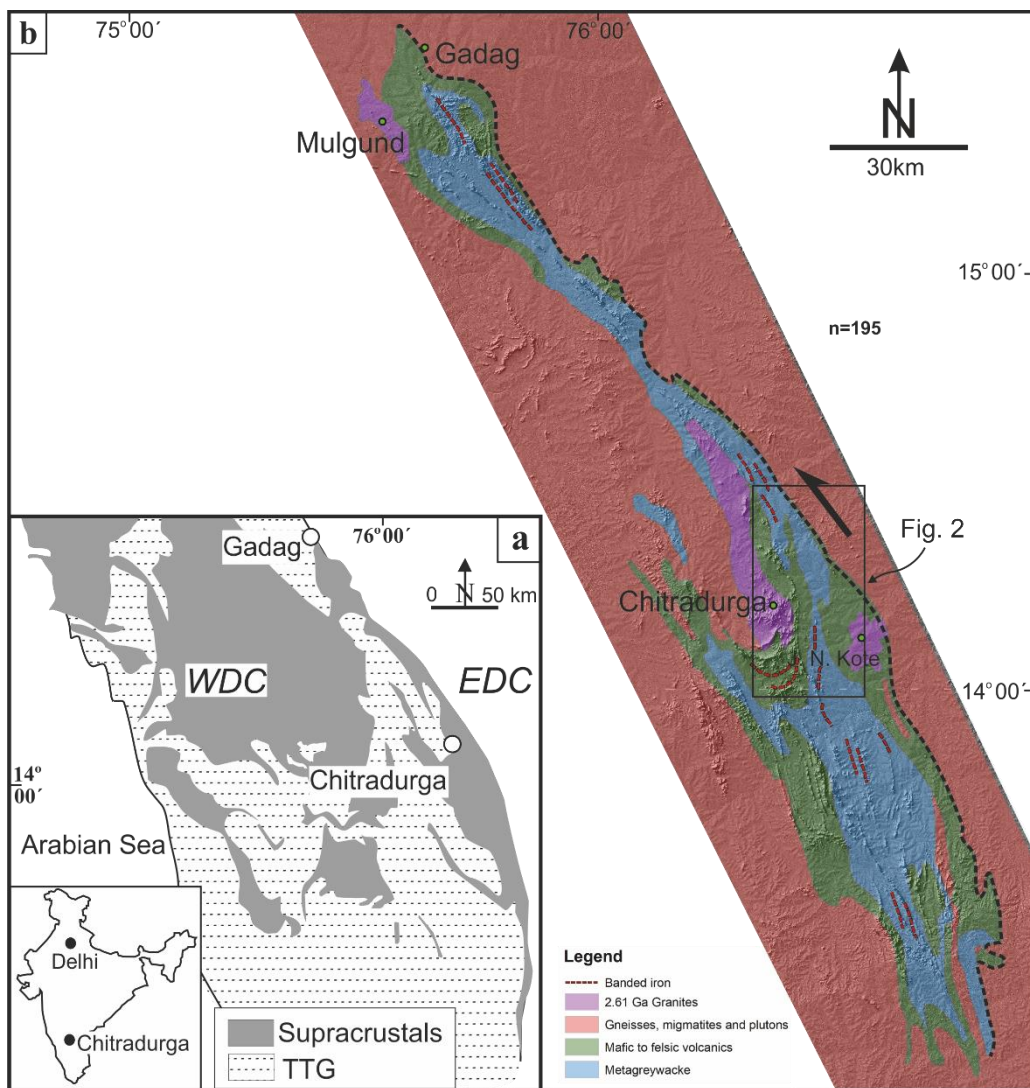
Figures:

Figure 01: (a) Regional map of western Dharwar craton, South Indian Shield [after Chadwick et al., 2003]. Inset shows the map of India. EDC = Eastern Dharwar Craton; WDC = Western Dharwar Craton; (b) Regional geological map (DEM) of the Chitradurga Schist Belt [modified after Jayananda et al., 2013]. Dotted line (in b) marks the eastern boundary of the Chitradurga Schist Belt, representing the Chitradurga Shear Zone (CSZ). Rectangular box near Chitradurga demarcates the study area.
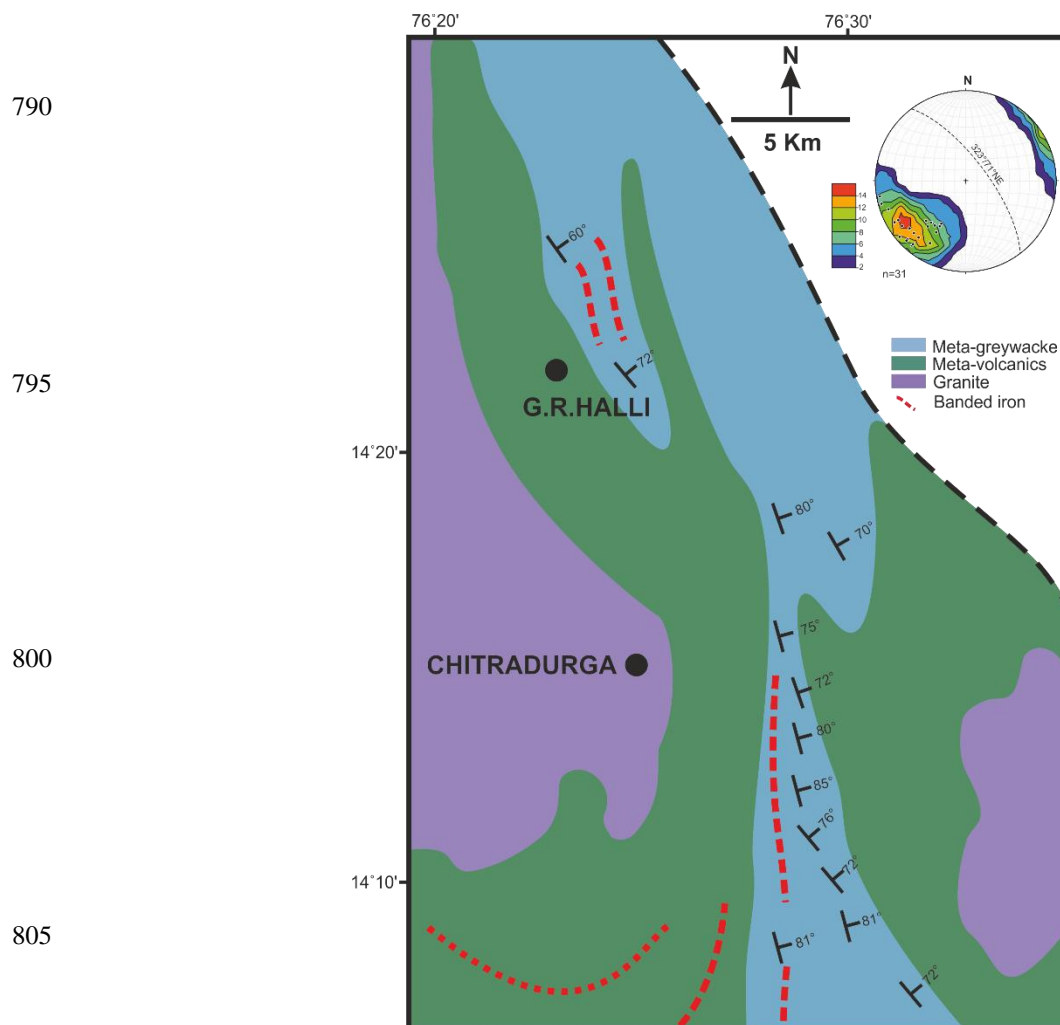
Figure: 02: .Geological map of the study area showing the foliation trends of the supracrustals. Lower hemisphere equal area projection shows the pole to foliation planes recorded from the region. Note that the mean foliation (dotted great circle) is 323º/71ºNE which is parallel to the CSZ (n= number data).Color scheme of the legend indicates variation in the contour density.

Figure 03. Field photographs from the study area. (a) Criss-cross orientation of quartz veins in metabasalt (camera towards E). (b) Close-up of a quartz vein in metabasalt showing crystal growth direction perpendicular to the vein wall (camera towards NE). (c) Cross-cutting nature in quartz veins showing dextral displacement (marked by yellow half-arrows; (camera towards N). (d) Wing cracks filled up with quartz veins associated with sinistral shearing (marked by yellow arrow; camera towards E).(e) NE dipping quartz vein showing slickenside lineations (maximum width recorded=120 cm), inset showing close up of the fault plane found in e. Marker pen placed along the orientation of the slickenside lineations. (f) Angular chunks of metabasalt (enclaves) enclosed within faulted quartz vein (camera towards NE). Dotted red line demarcates the enclave boundaries. Black arrow marks the slickenside lineation on the fault plane. (g)Fault planes in metabasalt showing congruous steps (marked by yellow arrow; camera towards E).
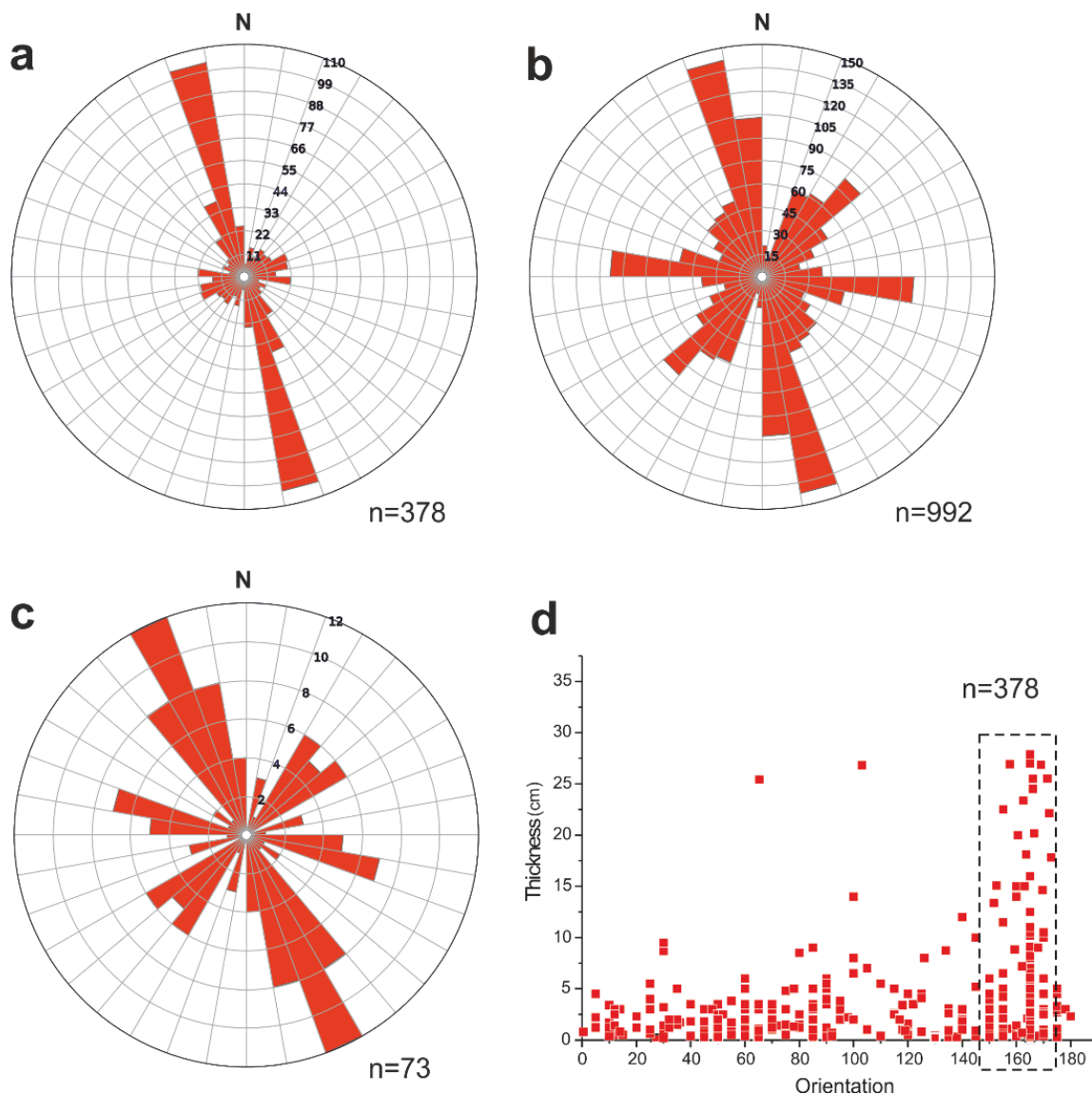
Figure 04. Rose diagrams and graphs of structural data recorded from the study area. (a), (b) and (c) are the rose diagrams of the strike orientation of the quartz veins, fractures and fault planes respectively. Note that the veins are mostly NNW-SSE striking whereas the fractures and fault planes show variable orientations, with a NNW-SSE maxima and a WNW-ESE to NE-SW sub maxima. (d) Graph of vein orientation vs. thickness, showing maximum vein thickness along NNW-SSE (marked with orange box). n= number of data.
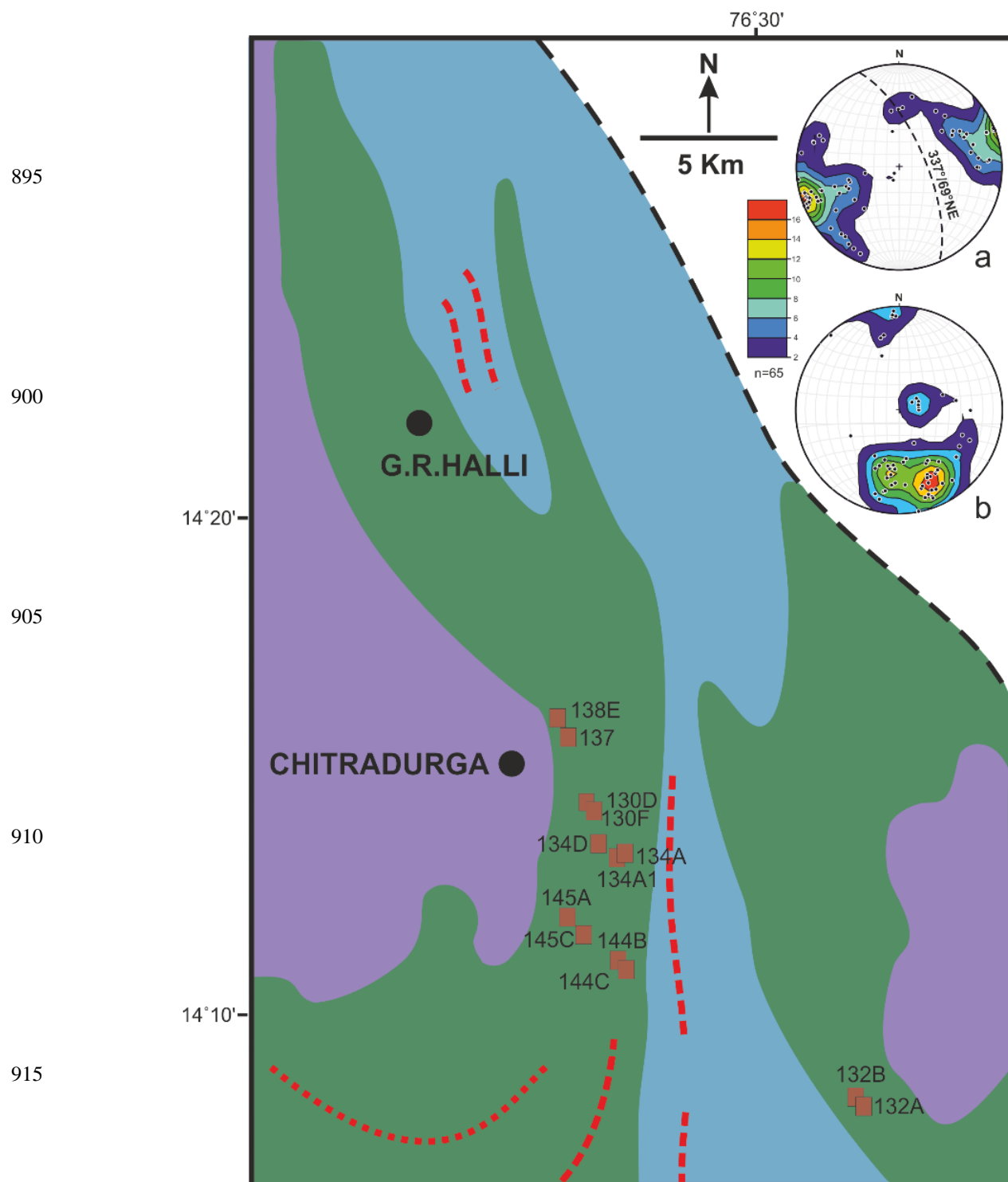
Figure 05. Map showing the location points (marked with brown boxes) from which oriented metabasalt
samples for AMS analysis have been collected. (a) Lower hemisphere equal area projection of poles (K_3)
to magnetic foliation (K_1K_2) plane. Mean orientation of K_1K_2 plane (dashed great circle)= 337°/69°E (b)
Lower hemisphere equal area projection showing the distribution of magnetic lineation (K_1).Color
scheme of the legend indicates variation in the contour density.

Figure 06. Tensile strength determination of metabasalt samples. (a) Sample cores for Brazillian tensile
strength (BTS) determination. Diameter: length=2:1. (b) Instruments used for measuring BTS. (c) Sample
cores obtained after failure.

955

960

965

970

975

980
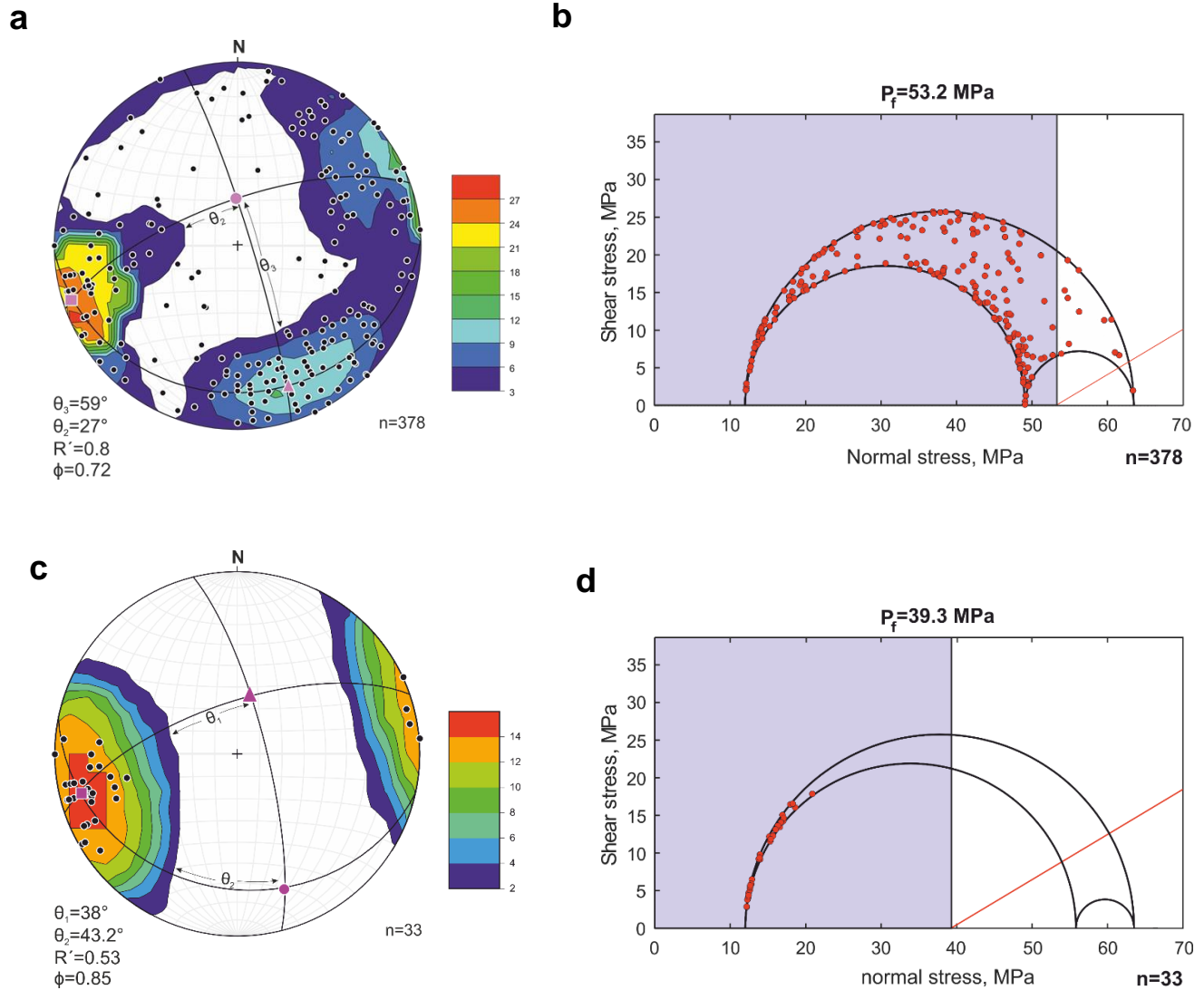
Figure 07.The state of stresses and fluid pressure (P_f) conditions determined from vein orientation data in the study area. (a) Lower hemisphere equal area projection of pole to veins shows girdle distribution, implying $P_f > \sigma_2$ (following Jolly and Sanderson, 1997). The empty space devoid of any vein pole data helps to determine the position of σ_1 (using Bingham statistics of the Stereonet 9 software) and thereby defines $\sigma_1\sigma_2$ and $\sigma_1\sigma_3$ planes. Angles θ_2 and θ_3 are measured which are used to determine the stress ratio (ϕ) and driving pressure ratio (R´) respectively. Color scheme of the legends indicate variation in the

contour density. Pink circle (σ_1), pink triangle (σ_2) and pink square (σ_3) respectively.(b) 3D Mohr circle diagram for high P_f conditions. Red line in the Mohr circle represents the reactivation envelope for cohesionless fractures. Vein pole data lying within the blue zone, i.e., to the left of the P_f (black) line

990 represent fractures filled up with veins that are susceptible to reactivate (Fractend code available via Github, 2017). (c) Lower hemisphere equal area projection of poles to vein data forming the SW cluster in (a), this cluster distribution of vein pole data indicate $P_f<\sigma_2$. Cluster maxima defines σ_3 axis. Angles θ_1 and θ_2 are measured and similarly ϕ and R' are determined. (d) 3D Mohr circle diagram for low P_f condition. Only a limited range of fracture filled up with veins are susceptible to reactivate. Red dots

995 represent pole to vein data, red line forms the reactivation envelope for cohesionless fractures.

1000

1005

1010

1015

1020

1025

1030
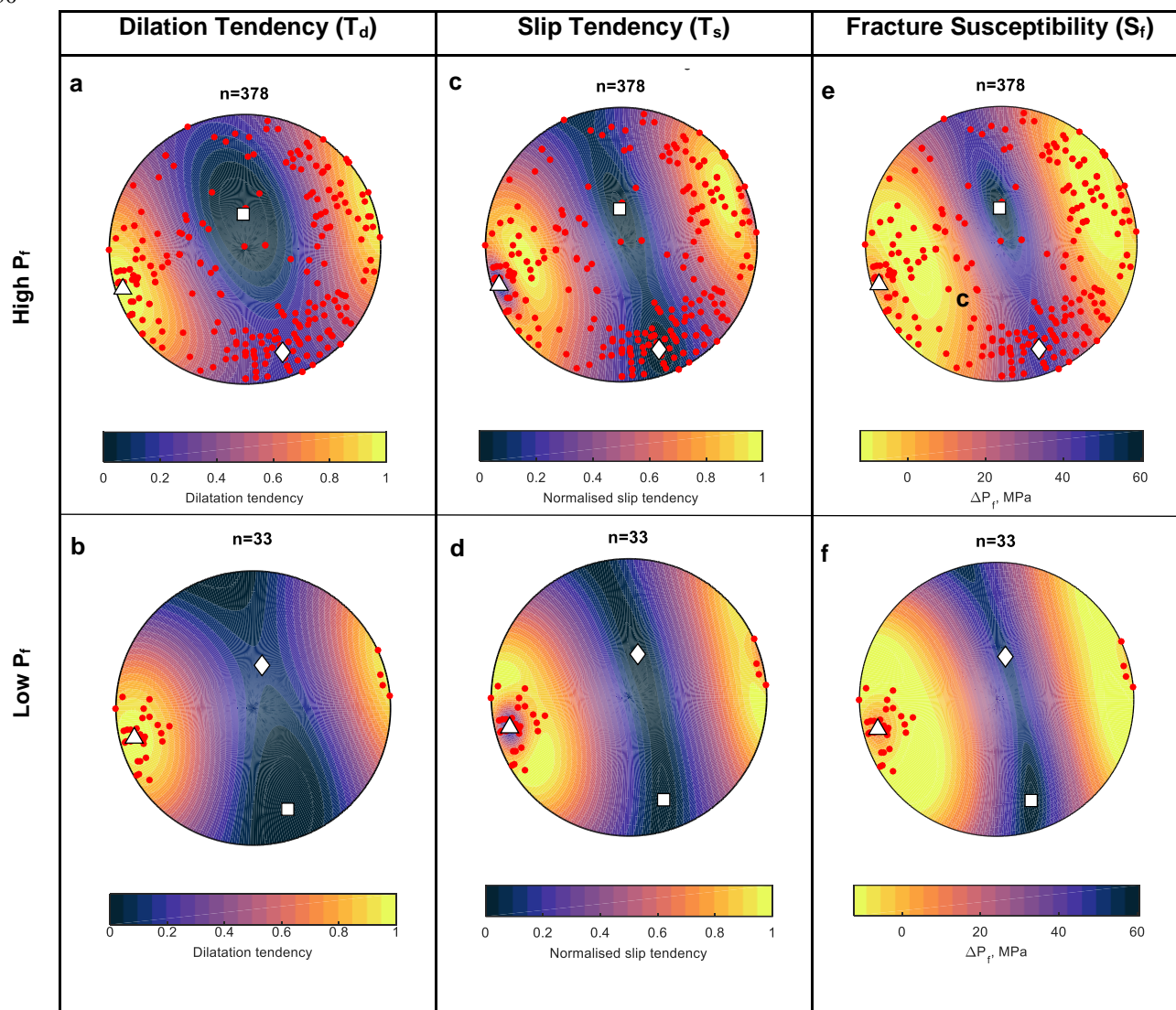
Figure 08.Lower hemisphere equal area projection for dilation tendency, slip tendency and fracture susceptibility in a given fluid pressure condition and for a specific stress state (Fractend code available via Github, 2017). (a) and (b) represents dilation tendency for high and low P_f. (c) and (d) represents slip tendency for high and low P_f. (e) and (f) fracture susceptibility for high and low P_f conditions respectively. Warm color zones in (a) and (b), represents vein orientations with higher propensity for tensional opening. In (c) and (d) warm colors indicate vein attitudes that suffered shearing. In (e) and (f) the warm color

zones stand for vein attitudes that are more susceptible to reactivate under low P$_f$ variation. 'Thermal'
1040   color scheme from Thyng et al., 2016. White square (σ$_1$), white diamond (σ$_2$) and white triangle (σ$_3$).

1045

1050   **Figure 09**. Paleostress analysis (using right dihedron method) of faults recorded in the metabasalts of the
study area; for both left lateral and right lateral normal faults. Red arrow marks the extension direction
(σ$_3$) and pink arrow marks the principal compression direction. The histogram shows the minimum values
for counting deviation. *n* and *nt* are the number of data accepted for tensor calculation and total number
of data respectively. R (stress ratio) = (σ$_2$-σ$_3$) / (σ$_1$-σ$_3$). Rose diagrams for fault plane strike, dip and plunge
1055   variations are also presented in the top right corner. 3D Mohr diagrams demonstrate possible areas of
fault reactivation with variation in susceptibility, colored circles represent pole to the fault planes. The
failure envelope for Mohr's circle is based on Byerlee (1978) initial friction angle of 16.7^0. Note that the
maximum extension is along NNE-SSW direction.

1060
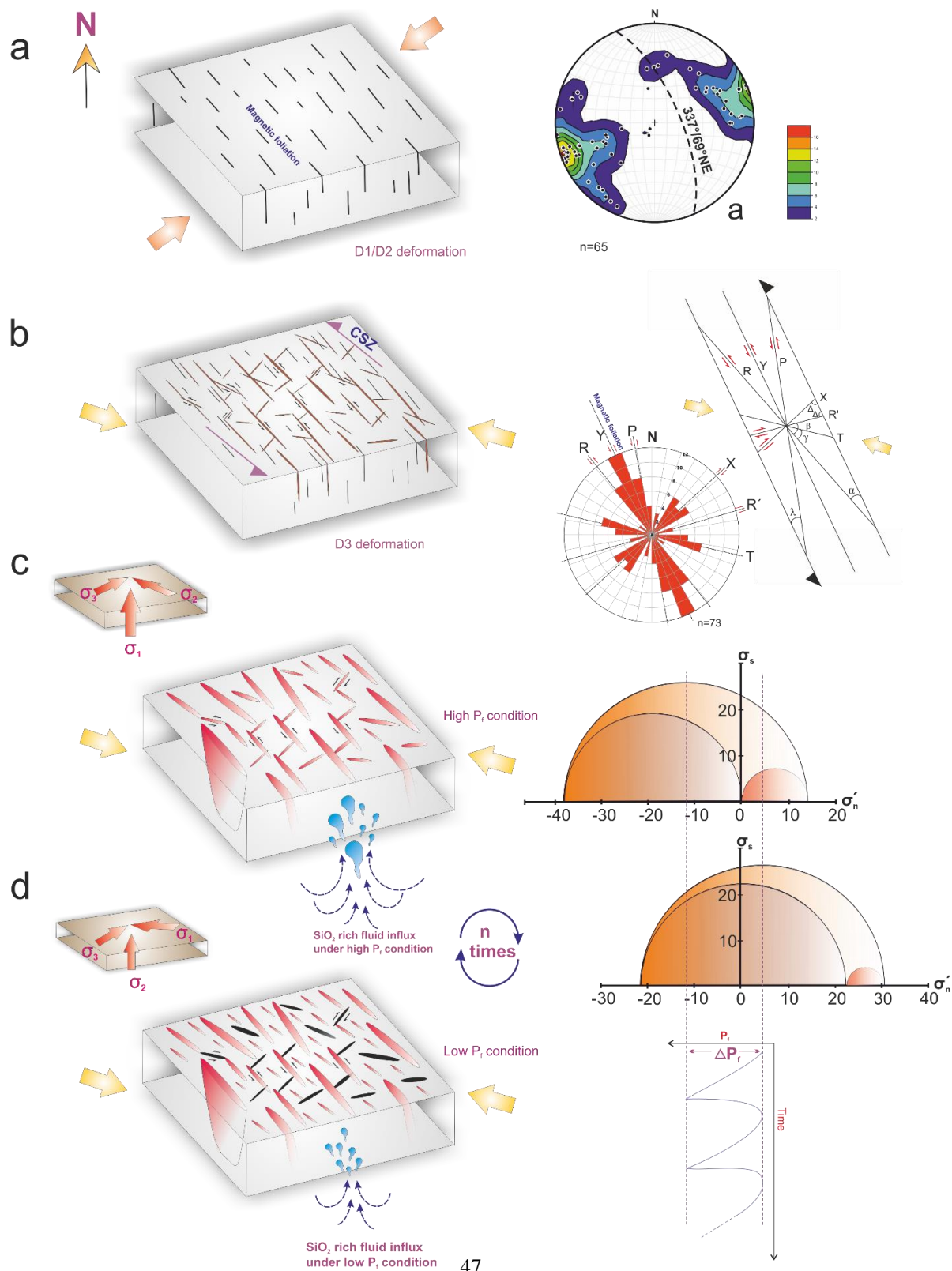
Figure 10.Schematic model showing formation and reactivation of fractures, along with vein
emplacement in the metabasalt host rock. (a) Development of the NNW-SSE to NW-SE oriented magnetic
fabrics in the rock unit under a NE-SW shortening related to D1/D2 deformation. Lower hemisphere equal
area projection shows mean orientation of the magnetic fabric ~ 337°/69°NE. (b) Formation of the Y, P,
R, R´, X and T shears related to the riedel shear system under a NW-SE to E-W shortening related to the
late D3 deformation (half arrows representing the shear zone boundary). The angles (α, β, γ, λ and Δ)
between the shear components are given after Logan et al. 1992. $\Phi=30°$ (angle of internal friction) is
measured from UCS studies of the samples from the study area. Corresponding riedel shear model, with
CSZ as the shear boundary and rose diagram showing orientations of the respective shear components.
(c) and (d) showing vein emplacement under high P_f and low P_f conditions respectively (state of stresses
along the fracture planes are given). Corresponding 3D-mohr circle diagrams quantifying the effective
normal stresses ($\sigma_n' = \sigma_n - P_f$; in Mpa) under both high and low P_f conditions, difference in P_f (ΔP_f ~13.9
MPa), obtained from the dashed lines representing the mean stress in each case. A conceptual graph shows
multiple cycles (n-times) of high and low P_f conditions in the study area justifying *fault-valve action* that
led to the emplacement of vein in the Chitradurga region.